Proliferation/Differentiation in intestinal organoids as a balance of ligand-modulated EGFR traffic

Caracci, MO[1*],Seidler, S, Muñoz-Nava, LM[1], Soetje, B[1], Michel, K[1], Bastiaens, PIH[1#].

[1]Department of Systemic Cell Biology, Max Planck Institute for Molecular Physiology, Dortmund, Germany

*Corresponding author

[#]Deceased

Summary

Expression and signaling competency at the plasma membrane of EGFR drives crypt proliferation vs villus differentiation by medium ligand-composition, aiding mouse intestinal organoids self-renewal and regeneration.

Abstract

Epidermal Growth factor (EGF) signaling is associated with (oncogenic) proliferation. Conversely, EGF-family ligands are able to trigger a differentiation program in cultured cells, an effect attributed to ligand affinity and EGFR phosphorylation. How EGF/EGFR driven proliferation-differentiation dynamics underlie tissue self-renewal has not been addressed. We show that culturing mouse small intestinal organoids (mSIOs) without EGF enhanced EGFR expression and base phosphorylation while maintaining a balanced development of proliferative crypts and differentiated villi. Addition of EGF or EREG triggers receptor endocytosis, reducing cell-surface and expression levels. While EGF promoted crypt proliferation, EREG promoted both proliferation and villus differentiation compared to untreated controls. Removal or re-introduction of EGF or EREG proved sufficient to induce development comparable to constant presence of ligands over 96h. Sub-saturating concentrations of EGF led to increased villus differentiation, resembling EREG treatments, suggesting that control over EGFR

34 endocytic cycle ultimately regulates the balance of proliferation and differentiation in
35 mSIOs

Introduction

Intestine morphology is characterized by differentiated enterocytes in the villus regions extending into the chyme for nutrient uptake, and a proliferative stem cell niche protected at bottom of crypts. Here, EGF/EGFR signaling is essential for maintance proliferation and self-renewal of the intestinal stem cells. Aberrant activity of EGF downstream signaling has been consistently associated with oncogenic transformations. EGF is a fundamental growth factor for many in vitro organoid culture systems (van der Vaart et al., 2021; Mahe et al., 2013; Wang et al., 2025; Hu et al., 2018). In mouse small intestinal organoids (mSIOs), Paneth cells secrete paracrine EGF within the stem cell niche in crypts (Sato et al., 2011a). Nevertheless, additional growth factors, including EGF, are added to the culture medium, mimicking the complexity of stromal compartment surrounding the intestinal epithelia (Sato et al., 2009).

EGFR is mainly expressed in the intestinal crypts (Yang et al., 2017) and inhibition of tyrosine kinase activity in mature organoids led to cell cycle arrest and quiescence of LGR5+ stem cells (Basak et al., 2017). EGFR inhibition also enhanced differentiation towards entero-endocrine cells, suggesting that perturbations to EGF/EGFR activation during distinct developmental stages could aid differentiation in mSIOs. Other EGF-family ligands such as NRG1, EREG and HB-EGF can replace EGF in mSIOs culture promoting organoid development (Lemmetyinen et al., 2023; Jardé et al., 2020; Chen et al., 2012), notably epithelial KO of NRG1 does not affect differentiation of secretory linage cells(Jardé et al., 2020). While NRG1 does not bind EGFR, EREG binds both EGFR and ERBB4 and has been used in human intestinal organoids to enhance cellular differentiation and crypt development (Childs et al., 2023).

Under basal medium conditions, mSIOs show both crypt proliferation and villus differentiation in two distinct, spatially separated compartments. In contrast, human intestinal organoids feature less cellular and structural diversity. Several remarkable efforts have been taken to enhance human organoid complexity by modulating cell signaling, including EGF inhibitors and EGF-family ligands. Nevertheless, the spatio-temporal responses of dynamic intracellular signaling networks to extracellular ligands

have been largely overlooked. (Yang et al., 2025; Fujii et al., 2018; Sato et al., 2011b; He et al., 2022).

It is well stablished that EGFR signaling plays an integral role in partially opposing phenotypic outcomes, including migration, apoptosis, proliferation and differentiation and is generally acknowledged that these responses are a result of different affinities among EGF-family ligands and their capacity to induce receptor phosphorylation (Abud et al., 2021; Jendrisek et al., 2026). For instance, high affinity ligands such as EGF, HB-EGF and TGFa, all produced in the intestinal epithelia, are often associated to cell proliferation. In other hand, low affinity ligands such as EREG and AREG, which are expressed by stromal cells in the intestine, are associated to cell differentiation and migration (Jendrisek et al., 2026; Lemmetyinen et al., 2023). Interestingly, EGF triggered responses are dependent on ligand concentration, where high, receptor saturating concentrations promote cellular proliferation while low, sub-saturating concentrations promote migratory behavior in cultured cells (Brüggemann et al., 2021; Joshi et al., 2023). The fact the EGF-EGFR signaling is able to trigger multiple phenotypical responses underscores the importance of this ligand-receptor pair in development. However, these properties have mainly been demonstrated in immortalized cell lines and this decision-taking has not yet been explored in complex tissues under homeorhetic conditions.

Therefore, we studied mSIOs in their early developmental stages during self-renewal and regeneration of seeded single crypts and their subsequent maturation. For this, we cultured mSIOs with either EGF or EREG to examine the differential effect of ligand availability on sustaining organoid crypt and villus development in aiding homeorhetic regeneration. We find that maintenance of plasma membrane (PM) EGFR localization drives villus development regardless of ligand affinity.

Results/Discussion

EGF promotes crypt proliferation and EREG promotes villus differentiation

102 In order to understand how the balance within crypt proliferation and villus
103 differentiation is triggered by distinct EGF-family growth factors we stained organoids
104 with CD44, a bonafide crypt marker (Sumigray et al., 2018), and enterocyte marker
105 AldoB to identify the differentiated villus region (Serra et al., 2019). Images were
106 acquired by CLSM and maximum intensity projections from multiple confocal stacks
107 were masked and quantified for area, as surrogates for crypt and villus growth
108 triggered by our treatments (Figure 1A and B). Intestinal organoid crypts were grown
109 for 96h in control NR medium (Noggin, R-SPO1) or NR medium supplemented with
110 either EGF (50 ng/mL), EREG (50 ng/mL). EGF and EREG as high and low affinity
111 ligands of EGFR respectively, are known to induce receptor phosphorylation and
112 endocytosis (Freed et al., 2017).
113
114 EGF and EREG addition significantly enhanced Organoid growth compared to NR
115 medium, however, Crypt Area was differentially enhanced by EGF, while Crypt and
116 Villus area was enhanced by EREG (Figure 1C) The relative ratio of Crypt-to-Villus
117 (CD44/ALDO) showed that EGF strongly favored the Crypt proliferation over Villus
118 differentiation, while NR medium and EREG maintained balanced development of
119 Crypt and Villus, despite the overall larger size of EREG treated organoids relative to
120 NR treatment (Figure 1D).
121
122 Crypt number was also greatly enhanced by EGF, while EREG only had small effect
123 in increasing the number of crypts relative to NR organoids (Figure S1A). Crypt
124 establishment is a direct result of apical constriction by Paneth cells(Langlands et al.,
125 2016). Paneth cells are found in the crypt, interspaced between Intestinal Stem cells
126 (ISCs) and their abundance is often correlated to ISCs numbers (Tallapragada et al.,
127 2021). Immuno-fluorescence staining showed that neither EGF or EREG enhanced
128 the number of Paneth cell, regardless of the effect observed in crypt area (Figure S1B).
129
130 Results suggests that both EGF and EREG are capable of inducing organoid
131 development through distinctive regulation of the proliferation/differentiation balance
132 with EGF promoting CD44+ crypts enlargement over differentiation into ALDO+ villus
133 region. On the other hand, EREG promotes growth of both crypt and villus regions,
134 thus suggesting that EGF-family ligands promote mSIOs development through
135 distinctive downstream mechanisms.

136

137 EGF and EREG mediated endocytosis reduces EGFR PM localization and expression.

138

139 EGF and EREG are known to bind, induce endocytosis and phosphorylation of EGFR.
140 EREG is also a ligand of ERBB4, however expression of this receptor is not detected
141 in small intestinal epithelia or stroma (Lemmetyinen et al., 2023). Saturating EGF
142 concentrations are commonly used in Organoid culture (Shankaran et al., 2021)at
143 which most of the PM receptor is internalized and undergo lysosomal degradation as
144 demonstrated in cultured immortalized cells (Brüggemann et al., 2021). In contrast,
145 EREG binding to EGFR promotes recycling back to the plasma membrane (Roepstorff
146 et al., 2009). In order to quantify end-point surface levels of EGFR, organoids were
147 incubated for 30 min with 50 ng/mL of EGF-647 before fixation and staining (Figure
148 1E). We observe that most of the internalized EGF-647 is located in the crypt regions
149 with few vesicles being observable in the villus regions, this is consistent with the
150 literature stating that EGFR is highly expressed in cycling cells within the intestinal
151 crypt (Yang et al., 2017). EGF-647 endocytosis was observed in organoids grown in
152 NR or EREG medium, organoids grown with unlabeled EGF for 96h showed very low
153 endocytosis suggesting reduced levels of PM EGFR (Figure 1F). Absence of ligands
154 allowed for accumulation of surface EGFR throughout the 96h developmental window
155 and EREG mediumted recycling back to the plasma membrane maintained high
156 surface levels.

157

158 EGF-647 endocytosis showed co-localization with late endosome marker Rab7
159 consistent with the use of saturating amounts of ligand (Figure 1F; Figure S2A and B).
160 DLS (Digital Lightsheet) imaging of EGF-647 endocytosis shows an initial association
161 to the crypts basal membrane followed by the entrance of vesicles travelling adjacent
162 to the inner membranes towards the apical side (Figure S2C and Video1). While basal
163 to apical trafficking is clearly observed we cannot discard the possibility of apical
164 endocytosis of EGF-647 from the lumen, as cell extrusions within the crypts are
165 observable in the time frame of our experiments which could allow EGF-647 to seep
166 into the luminal compartment. Transcytosis of EGF from basal to apical has been
167 proposed in MDCK epithelial layers (Brändli et al., 1991), however little is known of
168 the mechanisms involved

169

170 As a PM receptor, EGFR phosphorylation is highly dependent on its interaction with
171 ligands in the extracellular medium, nevertheless gene amplification enhancing
172 expression levels or point mutations affecting inhibitory mechanisms can lead to EGFR
173 phosphorylation in absence of ligand (Stanoev et al., 2018; Arteaga and Engelman,
174 2014). Immunoblotting of both total and phosphorylated EGFR Y1068 showed that
175 EGF and EREG grown organoids had a significant reduction in EGFR protein
176 expression compared to NR grown organoids (Figure 1G). Immuno-fluorescence
177 staining pEGFR Y1068 and CD44 after treatments, showing an increase in
178 phosphorylation staining only in crypts growth without EGF or EREG while organoid
179 grown with either ligand showed reduced staining (Figure 1H).
180
181 EGFR endocytic cycle is fundamental to regulate receptor phosphorylation, allowing
182 for degradation in late endosomes or the interaction with protein tyrosine
183 phosphatases (PTPs) within endomembrane compartments (Baumdick et al., 2015;
184 Joshi et al., 2023; Stanoev et al., 2018). In turn, NR grown organoids show an
185 accumulation of pEGFR likely due to endogenously expressed EGF by Paneth cells
186 and amplification by autocatalytic activation of PM bound receptors. It is important to
187 consider that medium changes every 48h imply 2 “pulses” of fresh EGF or EREG in a
188 96h developmental window, in between pulses, biosynthetic and endocytic
189 mechanisms allow for the replenishment of surface EGFR (Scharaw et al.,
190 2016).Surprisingly while EREG treatment did allow for significantly higher EGFR PM
191 levels, total levels were greatly diminished, despite this ligand promoting receptor
192 recycling over late endosome trafficking (Figure 1G and H).
193
194 <u>Temporal modulation of EGF-family ligands during development alters villus</u>
195 <u>differentiation</u>
196
197 In vitro cell culture often promotes proliferating conditions which ultimately allow for
198 biomass expansion required for biochemical assays, and organoid culture is no
199 exception. In the conception of ENR medium, addition of EGF and R-SPO1 were
200 sufficient to induce organoid growth from single crypts and the addition of Noggin
201 proved instrumental for organoid passaging over time (Sato et al., 2009). While lower
202 concentrations of EGF (e.g 10 ng/mL) were also tested in this seminal work with similar

203 results, little consideration was given to organoid developmental paths under evolving
204 availability of EGF in regards to ligand concentration or duration of stimuli.
205
206 To test the temporal requirements of EGF/EGFR signaling in organoid development,
207 organoids were grown for 96h with either EGF or EREG. However a complete medium
208 exchange with NR medium (No EGF or EREG) was done after 1h or after 48h of
209 incubation (Figure 2A). Developing from single crypts, organoids activate a
210 regeneration program that initially drives proliferation into a fetal-like state where
211 differentiation and stem cells markers are mostly absent (Sprangers et al., 2021),
212 budding within the organoid usually appears at the 48h mark where mature crypts will
213 develop (Sato et al., 2009) (Figure S3A). After 48h in culture, most organoids feature
214 a round morphology that is entirely CD44 positive, consistent with an undifferentiated
215 proliferating organoid (Serra et al., 2019). About 25% of them showed AldoB staining,
216 suggesting initial establishment of a villus region. The percentage of organoids
217 showing AldoB staining increases with EREG treated crypts, as shown for 96h
218 organoids grown with EREG. Overall, total area of organoids was not changed in any
219 of the treatments regardless of presence or absence of AldoB staining (Figure S3B-
220 E). EGF-647 endocytosis was also clearly observed in NR and EREG grown organoids
221 but not in EGF grown organoids as shown for 96h organoids. Endocytosis was
222 possible in organoids displaying either crypt or round morphology, often confined to
223 proliferating cells as noted by Ki67 staining (Figure S3F).
224
225 Regardless of EGF or EREG removal time-frame, organoids showed comparable total
226 area after 96h in culture. Moreover, 1h and 48h of EGF containing medium was
227 sufficient to induce crypt growth comparable to 96h with constant EGF. EREG induced
228 villus differentiation showed a similar trend as EGF with crypt development.
229 Surprisingly, 1h EGF treatment not only induced crypt growth, but also enhanced villus
230 differentiation to levels similar to the ones observed in EREG treatment (Figure2B and
231 C). Removal of EGF or EREG did not affect crypt number, however, removal of EGF
232 increased Paneth cell number compared to 96h control (FigureS1C and D).
233 Alternatively, organoids were treated for 96h and 1h with 50ng/mL of NRG1 (Figure
234 S1I), An EGF-family ligand know to bind ERBB3 and ERBB4 but not EGFR. NRG1
235 was able to induce organoid growth as previously shown (Jardé et al., 2020;
236 Lemmetyinen et al., 2023). Notably, 1h treatment with NRG1 and subsequent

237 withdrawal failed to induce organoid growth to 96h levels, with a significant growth-
238 increase relative to NR-grown organoids (Figure S1J and K). Therefore EGFR is likely
239 to induce robust signaling responses under EGF and EREG treatments.
240
241 96h and 48h incubation with EGF led to a near complete depletion of surface EGFR,
242 as very low EGF-647 endocytosis was detected., In contrast, 1h incubation with EGF
243 exhibited high levels of endocytosis suggesting high levels of surface EGFR, similar
244 to EREG treatments which increased over EREG-starvation times (Figure 2D). EGFR
245 phosphorylation was enhanced by EGF or EREG removal compared to the 96h
246 treatments further highlighting that phosphorylation of EGFR requires PM localization
247 (Figure S1E).
248
249 In a complementary experiment, single crypts were seeded in NR medium and then
250 ligands were re-introduced after 48h or 1h of growth factor starvation. (Figure 2E).
251 EGF and EREG-containing medium increased organoids total area and crypt area. In
252 contrast to early EREG treatment, addition of EREG after growth factor starvation
253 enhanced crypt growth similar to EGF and at the same time increased villus growth as
254 previously established (Figure 2F-G). Likewise, there was a marked increase in the
255 number of organoids featuring multiple crypts, although only EGF treatment enhanced
256 the number of Paneth cells (Figure S1F and G).
257
258 As previously shown, EGF and EREG reintroduction into the culture medium greatly
259 reduced endocytosis of labelled EGF-647 with EREG treated organoids retaining
260 some endocytic capacity consistent with EGFR recycling towards the plasma
261 membrane (Figure 2H). EGF or EREG removal from the culture medium allowed for
262 increased phosphorylation of EGFR, likewise, re- introducing EGF or EREG at 48h
263 after seeding significantly reduced phosphorylation, while brief 1h starvation did not
264 change phosphorylation levels compared to the NR condition (Figure S1H).
265
266 Altogether, these results highlight the remarkable robustness of EGFR signaling in
267 response to high affinity and low affinity ligands, effect that could not be replicated by
268 NRG1 treatment, which does not bind EGFR. EGF or EREG treatment at any point
269 tested was able to reduce EGFR surface levels compared to NR and lead to similar

270 total area growth, with 1h treatments upon seeding being sufficient to induce crypt and
271 villus development respectively.
272
273 Sub-saturating concentrations of EGF enhance both crypt proliferation and villus
274 differentiation
275
276 Given that organoids can develop in EGF-free medium, albeit at smaller size of crypt
277 and villus; and that EREG, a low affinity ligand of EGFR, induces organoid
278 development while maintaining high levels of surface EGFR, we tested if lower, non-
279 saturating concentrations of EGF could sustain organoid growth. Single crypts were
280 cultured for 96h with EGF concentrations decreasing by one order of magnitude of
281 starting at 50 ng/mL to 0.05 ng/mL (Figure 3A). NR treatment (0 ng/mL of EGF) showed
282 consistent development compared to 50 ng/mL as shown in previous experiments,
283 however, concentrations in between showed remarkable differences in development.
284
285 All EGF treatments enhanced organoid total area compared to NR, however crypt
286 growth was significantly enhanced starting at 0.5 ng/mL. Notably, villus differentiation
287 was increased starting at 0.05 ng/mL before being reduced at 50 ng/mL (Figure 3B).
288 Likewise, CD44/ALDO ratio was enhanced towards crypt development starting at 0.5
289 ng/mL and increased at 50ng/mL as villus area is reduced (Figure 3C).
290
291 EGF-647 endocytosis also showed a negative correlation between surface EGFR and
292 EGF concentration. Notably, concentrations that enhanced villus development showed
293 surface EGFR levels similar to EREG treatments (Figure 3D).
294
295 Multiple pulses of EGF deplete EGFR surface expression reducing villus differentiation
296
297 Removing saturating amounts of EGF from the culture medium, EREG treatment and
298 sub-saturating EGF concentration all are able to maintain a high level of surface EGFR
299 expression compared to long term EGF treatment. A combination of biosynthesis and
300 endocytic cycling is constantly supplying EGFR to the cell surface, EGF has also been
301 shown to increase EGFR mRNA levels (Scharaw et al., 2016), thus constant turnover
302 is likely critical for the phenotypical outcomes we observe.
303

304 To further test this idea, organoids were grown for 96h, however medium was
305 exchanged only 1, 2 or 4 times during this time window in order to constantly deplete
306 surface EGFR in developing organoids (Figure 4A). Total Area of the organoids
307 remained unchanged in EGF and EREG regardless of the number of medium
308 changes, showing that fresh medium addition does not change overall organoid
309 growth (Figure 4B). Contrastingly, Crypt area was increased while Villus area was
310 reduced by multiple EGF medium changes, an effect that was not observed with EREG
311 treatment that maintained Crypt Area in all treatments. 4x EREG treatments
312 significantly reduced Villus Area compared to 96h and 48h, however this change did
313 not significantly affect Crypt/Villus balance (Figure 4C and D). As expected, multiple
314 EGF treatments greatly reduced EGF-647 endocytosis while EREG and NR
315 treatments maintained similar levels of endocytosis in all treatments (Figure 4E).
316
317 Concluding Remarks
318
319 Human plasma levels of EGF range between 0.04 and 0.1 ng/mL (Alshammari et al.,
320 2026), whereas, concentrations of up to 300 ng/mL have been identified in rodent milk
321 and is essential for early gastrointestinal development in newborns. After weaning and
322 with age, EGF levels in the intestine are greatly reduced (Schaudies et al., 1989;
323 Fisher and Lakshmanan, 1990). EGF expression is also upregulated in Paneth cells
324 upon injury in the intestinal epithelia (Calafiore et al., 2023). Absolute concentrations
325 of EGF in tissues could also be obscured by tissue geometry, such as the confined
326 space within an intestinal crypt, allowing for a higher concentration of ligand within a
327 lower volume (Tschumperlin et al., 2004; Schmick and Bastiaens, 2014) In all, the
328 intestinal tissue is exposed to changing of ligands throughout development, with higher
329 levels are often associated with epithelial regeneration processes interspersed within
330 long periods of normal proliferation and differentiation. In turn, periods of low ligand
331 availability enhance long term stability of EGFR expression and enrichment at the
332 plasma membrane, making intestinal crypts susceptible to changes in the
333 concentration of ligands in the environment.
334
335 Saturating amounts of EGF might be instrumental for passaging and expanding
336 intestinal organoids, especially in when seeding single stem cells (Boretto et al., 2024).
337 However, seeding single crypts allows for a pre-stablished cellular niche to trigger

338 initial organoid regeneration, even in the absence of medium EGF. Over 48h, the
339 organoids establish a fetal-like morphology which was not influenced by EGF or EREG
340 as organoids developed equally in total area regardless of presence or absence of
341 ligand. Similar developmental profiles could be induced by re-introducing EGF or
342 EREG after 48h and by removing ligands after 1h of incubation upon crypt seeding,
343 highlighting the robustness of EGFR mediated signaling.
344
345 To couple phenotype to EGFR activity, we incubated organoids with labelled EGF-647
346 and examined endocytosis as measurement of the amount of EGFR present in the
347 basolateral membrane after treatments. It is well established in the literature that
348 receptor-bound EGF is released under acidic pH of endosomal compartments.
349 Whether this applies to EREG and EREG-triggered recycling produces ligand-less
350 surface receptors is unknown. Labelled EGF has been extensively used to quantify
351 surface levels and/or total receptor levels in cell lines (Stanoev et al., 2018; Joshi et
352 al., 2023; Roepstorff et al., 2009).This process usually include incubations and washes
353 with ice-cold buffers. These treatments are not possible in organoids where cold
354 washes could compromise the integrity of the Matrigel matrix sustaining organoid
355 morphology and the intracellular cytoskeletal network.
356
357 While EGF treatment might promote receptor degradation, thus reducing EGFR
358 endocytosis of EGF-647, it is also possible that smaller vesicles associated to clathrin
359 mediated endocytosis of EGFR monomers could not be detectable by CLSM over the
360 background signal. In other hand, higher levels of surface receptor in NR and EREG
361 treatment enhance non-clathrin mediated endocytosis of EGFR clusters within larger
362 vesicles and higher number of fluorescent molecules which facilitate detection. On the
363 other hand EREG, a low affinity EGFR ligand that has been shown to promote
364 sustained EGFR phosphorylation and differentiation in cultured cells (Freed et al.,
365 2017). After 96h of growth we were unable to observe increased phosphorylation of
366 EGFR in EREG treated organoids, pEGFR levels quantified by immunofluorescence
367 were often comparable to EGF treated organoids, also total levels of EGFR were
368 reduced by EREG 96h treatment. EREG-induced EGFR endocytosis leads to rapid
369 recycling back to the plasma membrane and reduced ubiquitination compared to EGF
370 treatment, however, a fraction of EREG-bound receptors shows colocalization with

371 late endosomal markers (Roepstorff et al., 2009; Deguchi et al., 2024) which could
372 account for degradation.
373
374
375 ## Methods
376
377 Mouse intestinal organoids culture
378
379 AdDF+++ medium containing Advanced Dulbecco's modified Eagle's medium/F12
380 supplemented with 100 u/mL penicillin/streptomycin, 10 mM HEPES, 2mM Glutamax.
381 ENR medium consists of AdDF+++ supplemented with 1x B27 (Life Technologies) and
382 1.25 mM N-acetylcysteine, 50ng/mL mEGF (Peprotech, 315-09), 500 ng/mL R-
383 Spondin 1 (Peprotech, 315-32) and 100 ng/mL Noggin (Peprotech, 250-38).
384 Alternatively, medium without EGF was used as "NR medium". Cryopreserved mouse
385 small intestinal organoids were purchased form STEMCELL Technologies (Cat
386 #70931) and grown in Matrigel 30 μL droplets in 24 well plates in ENR medium for 96-
387 120h before splitting by mechanical disruption with yellow pipette tips. Alternatively for
388 treatments, NR medium was supplemented with 50 ng/mL of EREG (Biotechne, 1195-
389 EP-025,) or 50 ng/mL NRG1 (Biotechne-377-HB-050/CF).
390
391 Immuno-staining
392
393 Single organoid crypts were seeded in 20 μL Matrigel droplets in x-well culture
394 chambers 8 wells on coverslips (Sarstedt, 94.6190.802). After 96h of growth organoids
395 were fixed for 40 min in 4% PFA. Then washed 3 times with IF-buffer (0.2% Triton
396 X100, 0.05% Tween20) for 5 min and permeabilized with PBS 0.5% Triton X100 for
397 1h. Organoids were then blocked with IF-Buffer supplemented with 3% BSA.
398 Alternatively, for staining of phosphorylated EGFR (pEGFR), BSA was replaced by
399 50% Goat Serum (Invitrogen, 50197Z) and 50% IF buffer for both blocking and
400 antibody staining. Primary antibodies CD44 (1:500; BD Pharmigen™, 560568),
401 Lysozyme (1:1000, DAKO, A0099) and Aldolase (1:500, ab153828, Abcam), pEGFR
402 (1:250,EP774Y,Abcam), Ki-67 (1:500, 55060, BD Biosciences) , Rab7 (1:500, D95F2,
403 Cell Signaling Technology) were incubated overnight with agitation at 4°C. Organoids

404 were washed 3 times with IF Buffer for 5 min and then incubated for 1h with Alexa
405 Fluor secondary antibodies (1:500,Thermo-Fisher) and DAPI (1:1000). Alexa Fluor
406 488 (A11008, A11001), Alexa Fluor 546 (A11081, A11030) and Alexa Fluor 647
407 (A31573, A21247) secondary antibodies were used. After washing with IF buffer,
408 samples were kept in Clearing Solution (50% v/v Glycerol, 2.5M Fructose) up to
409 imaging.
410
411 Confocal Laser Scanning Microscopy (CLSM) imaging
412
413 Organoids were imaged using Leica Confocal TCS SP8 with a 20x/0.75 NA air
414 objective. 2 μm spaced z-stacks were acquired in the fluorescence channels suitable
415 for each sample. Area quantifications were performed using binary masks thresholded
416 from Maximum Intensity Projections of either DAPI, CD44 or AldoB representing total,
417 crypt and villus area respectively. Alternatively, organoid crypts were imaged with
418 63x1.4 NA oil-immersion objective for pEGFR and CD44 imaging.
419
420 EGF-647 endocytosis
421
422 The His-CBD-Intein-(Cys)-hEGF-(Cys) plasmid was kindly provided by Prof. Luc
423 Brunsveld, University of Technology, Eindhoven. EGF-647 was purified in house as
424 previously described (Sonntag et al., 2014; Joshi et al., 2023). For endocytosis in
425 organoids, medium was aspirated from x-well culture chambers, 8 wells on coverslips
426 (94.6190.802, Sarstedt) and rinsed with warm AdDF+++ once. Subsequently,
427 organoids were incubated for 30 min with 50ng/mL of EGF-647 before fixation with 4%
428 PFA. Organoids were imaged in Leica Confocal SP8 with 63x oil immersion objective,
429 crypts were identified by Ki-67 staining. Cellular area was masked with Ki67 and Rab7
430 staining and the number vesicles were quantified using the find maxima command in
431 Fiji.
432
433 Immunoblotting
434
435 Organoid samples were pelleted, resuspended in modified RIPA buffer (50 mM Tris
436 HCl, pH 7.4, 150 mM NaCl, 1 mM EDTA, 1 mM EGTA, 0.5% Triton X-100, and 0.5%

437 sodium deoxycholate) supplemented with Complete Mini EDTA-free protease inhibitor
438 (Roche Applied Science) and phosphatase inhibitor cocktail 2 and 3 (1:100, P5726
439 and P0044, Sigma–Aldrich), frozen in liquid nitrogen and stored in -70°C freezer.
440 Samples were then dissociated using 10-gauge needle syringes and centrifuged at
441 12,000 rpm for 15 min at 4°C. Protein concentration was determined by BCA (Thermo
442 Scientific, 23235) and 50 μg of protein was loaded in 8% SDS/PAGE gels and then
443 transferred into PVDF membranes. Membranes were then blocked in intercept buffer
444 and incubated with primary antibody overnight. EGF Receptor (C75B9) (1:1000, Cell
445 Signaling Technology, 2646) for total EGFR, EGFR Y1068 (AP774Y) (1:500; Abcam,
446 40815) for phospho EGFR (pEGFR), and α-Tubulin (1:10000; Merck, T6074,) were
447 used. Secondary antibodies IRDye 680 donkey anti-Rabbit IgG (1:10000), IRDye 800
448 donkey anti-Mouse IgG (1:10000) and IRDye 800 donkey anti-Rabbit IgG (1:10000)
449 (LI-COR Biosciences) were used.
450
451 Digital Lightsheet (DLS) Microscopy
452
453 Organoids were grown in U-Shaped Capillaries 20 x 1.5 mm (Leica, 158007061) inside
454 Glass-Bottom 35 mm MatTek Dishes (MatTek Life Sciences, P35G-1.5-10-C) for 96h
455 in NR medium. Before imaging, organoids were treated for 1h with 1:500 Cell Mask™
456 Green Actin Tracking stain (Invitrogen, A57243) and Hoechst 33342 (Invitrogen,
457 C10340 G). Afterwards organoids were washed twice with warm AdDF+++ medium
458 and returned to fresh NR medium. Organoids were imaged in Leica TCS SP8 Digital
459 Lightsheet (DLS) DMi850 using HC PL FLUOTAR 5x/0.15 excitation objective and
460 FLUOTAR L25x/0.95 W DLS detection objective. 50ng/mL of EGF-647 was added
461 after calibration and ROI selection.
462
463 Statistical Analyses
464
465 Analysis was performed with at least 3 biological replicates (N=3) unless otherwise
466 stated. Scatter plots show mean±95%CI and bar graphs show mean±SD. For single
467 group comparisons Krustal-Wallis with Dunn's multiple comparisons test was used.
468 For multiple group comparisons Two-way ANOVA with Sidak's multiple comparisons

test multiple comparisons test. p-values <0.05 are shown. All analyses and graphs were implemented using Prism GraphPad

Acknowledgments

This project was supported by Max Planck Society for the Advancement of Science. We thank Dr. Malte Schmick for invaluable comments in the production of this manuscript. Special thanks to Dr. Sven Müller for technical support with confocal and DLS microscopy. Figure 1E was created with BioRender.com.

MOC: conceptualization, data curation, formal analysis, experimental methodology, visualization, writing and editing, SS: experimental methodology, editing, LMMN: conceptualization, writing and editing, BS: conceptualization, data curation, visualization, editing, KM: experimental methodology, editing. PHIB: Conceptualization, funding acquisition, supervision, project administration.

Prof. Dr. Philippe I.H. Bastiaens, passed away on May 15, 2025. All authors agree that his inclusion as a co-author is appropriate to honor his intellectual contribution to this work.

The authors state that this research was conducted in the absence of any commercial or financial relationships that could be construed as a potential conflict of interest.

Figure 1. EGFR surface depletion by EGF promotes Crypt proliferation while EREG promotes both proliferation and differentiation. (A) Maximum intensity projections (top) were binarized (bottom) to quantify the area of DAPI (nuclei, blue), CD44 (Green) and AldolaseB (Magenta) used to quantify "Total", "Crypt" and "Villus" area respectively (B-H) Organoids were grown, with NR medium or supplemented with either EGF (50ng/mL) or EREG (50ng/mL) for 96h with a complete medium change at 48h. (B) Organoids were immuno-stained with CD44 (Green) AldoB (Magenta) and DAPI (Blue). Scale Bar 100 μm. (C) Quantification of the areas as shown in (A). Scatter plots with mean±95%CI. N=3; n=57-67 organoids/condition; significance was calculated by Kruskal-Wallis with Dunn's multiple comparisons test. p-values <0.05 are shown (D) Relative ratio of CD44 to ALDO areas from (C). Scatter plot with mean±95%CI; significance was calculated by Kruskal-Wallis with Dunn's multiple comparisons test. p-values <0.05 are shown. Values above 1 suggests organoid development tends towards crypt proliferation while values below 1 tend to villus differentiation (E) Alexa Fluor-647 labelled EGF (50 ng/mL) is added to organoids after 96h of growth, after 30 min of incubation organoids were fixed and stained. Alexa Fluor-647 positive endosomes indicate the level of surface EGFR and consecutive endocytosis upon ligand binding. (F) (Left) Representative micrographs of organoids after immunofluorescence staining against Ki67 (Yellow) and Rab7 (Magenta). EGF-647 internalized through EGFR endocytosis is labelled in (Green). Scale bar 20μm. (Right) EGF-647 vesicles per area as scatter plots mean±95%CI; N=3, n=28-37 crypts/condition; significance was calculated by Kruskal-Wallis with Dunn's multiple comparisons test. p-values <0.05 are shown. (G) (Left) Immunoblot of pEGFR, EGFR and a-TUB with approximate MW in kDa. (Right) Bar Graphs of mean±SD of pEGFR or EGFR relative to a-TUB. N=4. (H) (Left) Ratio of pEGFR to CD44 Scatter plots of mean±95%CI. N=3, n=32-60 crypts/condition; significance was calculated by Kruskal-Wallis with Dunn's multiple comparisons test. p-values <0.05 are shown. (Right) Representative micrographs of organoids after immunofluorescence staining against pEGFR (top) and CD44 (bottom). Scale bar 20μm.

Figure 2. Removing EGF or EREG after crypt seeding does not modify developmental trayectories. (A-D) Organoids were grown, with NR medium supplemented with either EGF (50ng/mL) or EREG (50ng/mL) for 48h or 1h, then complete medium was

replaced with NR medium until fixation at 96h. (B) Scatter plots showing mean±95%CI, N=3, n=57-79 organoids/condition of masked Total, CD44+ and ALDO+ areas. Significance was calculated by Two-way ANOVA and Sidak's multiple comparisons test multiple comparisons test. p-values <0.05 are shown. (C) Relative ratio of CD44 to ALDO areas from (B). Scatter plot mean±95%CI of relative ratio within CD44/ALDO areas. Values above 1 suggests organoid development tends towards crypt proliferation while values below 1 tend to villus differentiation. Significance was calculated by Two-way ANOVA and Sidak's multiple comparisons test. p-values <0.05 are shown. (D) EGF-647 vesicles per area as scatter plots showing mean±95%CI; N=3, n=28-41 crypts/condition; significance was calculated by Two-way ANOVA and Sidak's multiple comparisons test multiple comparisons test. p-values <0.05 are shown. (E-H) Organoids were grown for 1h and 48h with NR, then complete medium was replaced with NR medium supplemented with either EGF (50ng/mL) or EREG (50ng/mL). (F) Scatter plots showing mean±95%CI, N=3, n=57-73 organoids/condition of masked Total, CD44+ and ALDO+ areas. Significance was calculated by Two-way ANOVA and Sidak's multiple comparisons test multiple comparisons test. p-values <0.05 are shown, ns non-significant. (G) Relative ratio of CD44 to ALDO areas from (B). Scatter plot mean±95%CI of relative ratio within CD44/ALDO areas. Values above 1 suggests organoid development tends towards crypt proliferation while values below 1 tend to villus differentiation. Significance was calculated by Two-way ANOVA and Sidak's multiple comparisons test multiple comparisons test. p-values <0.05 are shown. (H) EGF-647 vesicles per area as scatter plots showing mean±95%CI; N=3, n=20-38 crypts/condition; significance was calculated by Two-way ANOVA and Sidak's multiple comparisons test multiple comparisons test. p-values <0.05 are shown.

Figure 3. Subsaturating concentrations of EGF trigger both crypt and villus growth. (A-D) Organoids were grown, with NR medium, supplemented with EGF at different concentrations: 50, 5, 0.5 and 0.05 ng/mL or EREG 50 ng/mL for 96h before fixation and immno-staining. (B) Scatter plots showing mean±95%CI, N=3, n=44-71 organoids per condition, significance was calculated by Kruskal-Wallis with Dunn's multiple comparisons test. p-values <0.05 are shown (C) Relative ratio of CD44 to ALDO areas from (B). Scatter plot mean±95%CI of relative ratio within CD44/ALDO areas. Values above 1 suggests organoid development tends towards crypt proliferation while values

below 1 tend to villus differentiation. significance was calculated by Kruskal-Wallis with Dunn's multiple comparisons test. p-values <0.05 are shown (D) EGF-647 vesicles per area as scatter plots showing mean±95%CI; N=3, n=39-48 crypts/condition; significance was calculated by Kruskal-Wallis with Dunn's multiple comparisons test. p-values <0.05 are shown

Figure 4. Multiple EGF or EREG medium changes reduces villus differentiation. (A-E) Organoids were grown, with NR medium or supplemented with either EGF (50ng/mL) or EREG (50ng/mL) for 96h with a complete medium change every 24h (4x), 48h (2x) or 96h (1x). (B-C) Scatter plots showing mean±95%CI, N=3, n=47-67 organoids/condition of masked areas corresponding to (B) total Area and (C) CD44+ and ALDO+ areas; significance was calculated by Two-way ANOVA and Sidak's multiple comparisons test multiple comparisons test. p-values <0.05 are shown. (D) Relative ratio of CD44 to ALDO areas from (C). Scatter plot mean±95%CI of relative ratio within CD44/ALDO areas. Values above 1 suggests organoid development tends towards crypt proliferation while values below 1 tend to villus differentiation. significance was calculated by Two-way ANOVA and Sidak's multiple comparisons test multiple comparisons test. p-values <0.05 are shown (E) EGF-647 vesicles per area as scatter plots showing mean±95%CI; N=3, n=21-40 crypts/condition; significance was calculated by Two-way ANOVA and Sidak's multiple comparisons test multiple comparisons test. p-values <0.05 are shown.

Figure S1. Effect of EGF/EREG temporal modulation in Crypt number, Paneth cell number and pEGFR staining. (A-B) Organoids were grown with NR medium or supplemented with either EGF (50ng/mL) or EREG (50ng/mL) for 96h with a complete medium change at 48h (A) Percentage of Organoids displaying either 1-2 or 3 or more crypts. N=3 (B) (Left) Organoids were immuno-stained with CD44 (Green) and Lysozyme (Lyz, Magenta). Scatter plots showing mean±95%CI of Paneth cells number per organoids was quantified in each condition. Quantification of n=43-56 organoids/condition, N=3, significance was calculated by Krustal-Wallis with Dunn's multiple comparisons test. p-values <0.05 are shown. (C-E) Organoids were grown, with NR medium supplemented with either EGF (50ng/mL) or EREG (50ng/mL) for 48h or 1h, then complete medium was replaced with NR medium until fixation at 96h.

(C) Percentage of Organoids displaying either 1-2 or 3 or more crypts. N=3 (D) Scatter plots showing mean±95%CI of Paneth cells number per organoids was quantified in each condition. Quantification of n=42-61 organoids per condition, N=3, significance was calculated by Two-way ANOVA and Sidak's multiple comparisons test multiple comparisons test. p-values <0.05 are shown (E) Ratio of pEGFR to CD44 Scatter plots of mean±95%CI. N=3, n=21-49 crypts/condition; significance was calculated by Two-way ANOVA and Sidak's multiple comparisons test multiple comparisons test. p-values <0.05 are shown. (F-H) Organoids were grown for 1h and 48h with NR, then complete medium was replaced with NR medium supplemented with either EGF (50ng/mL) or EREG (50ng/mL). (F) Percentage of Organoids displaying either 1-2 or 3 or more crypts. N=3 (G) Scatter plots showing mean±95%CI of Paneth cells number per organoids was quantified in each condition. Quantification of n=50-69 organoids/condition, N=3, significance was calculated by Two-way ANOVA and Sidak's multiple comparisons test multiple comparisons test. p-values <0.05 are shown (H) Ratio of pEGFR to CD44 Scatter plots of mean±95%CI. N=2-3, n=39-54 crypts/condition; significance was calculated by Two-way ANOVA and Sidak's multiple comparisons test multiple comparisons test. p-values <0.05 are shown. (I) Organoids were grown, with NR medium or NR medium supplemented with NRG1 (50ng/mL) for 96h or 1h. After 1h complete medium was replaced with NR medium until fixation at 96h. (J) Organoids were immuno-stained with CD44 (Green) AldoB (Magenta) and DAPI (Blue). Scale Bar 100 μm. (J-K) Scatter plots showing mean±95%CI of masked areas corresponding to total, CD44+, ALDO+ and ratio Quantification of n=58-65 organoids/condition, N=2-3, significance was calculated by Krustal-Wallis with Dunn's multiple comparisons test. p-values <0.05 are shown.

Figure S2. Organoids grown for 48h often display no villus region and retain EGF-647 endocytosis in proliferating cells. (A) Brightfield time lapse imaging of developing organoid from seeded crypts in EGF medium showing standard developmental trajectories between seeding (0h), 24h, 48h, and 96h (B) Organoids were grown, with NR medium or supplemented with either EGF (50ng/mL) or EREG (50ng/mL) for 48h before fixing and staining. (C) Percentage of Organoids showing ALDO+ villus region after 48h of development, N=3. (D) Scatter plots of masked areas corresponding to total area, for all organoids (Left) and organoids with ALDO+ region showing

mean±95%CI, N=3, n=45-70 organoids/condition, (Right). Quantification of, significance was calculated by Kruskal-Wallis with Dunn's multiple comparisons test. p-values <0.05 are shown, ns non-significant. (E) Organoids were immuno-stained with CD44 (Green) AldoB (Magenta) and DAPI (Blue). Organoids ALDO- and ALDO+ are shown for each treatment. Scale Bar 100 μm. (F) Alexa Fluor-647 labelled EGF (50ng/mL) is added to organoids after 48h of growth, after 30min of incubation organoids were fixed and stained with Ki67 (Yellow), Rab7 (Magenta) and DAPI (Blue). EGF-647 is show in (Green). Representative images of Round or Crypt morphologies are represented for each treatment.

Figure S3. EGF-647 endocytosis in organoid crypts co-localizes with late endosomal marker Rab7. (A-B) Organoids were grown, with NR medium or supplemented with either EGF (50ng/mL) or EREG (50ng/mL) for 96h with a complete medium change at 48h. (A) Organoids were immuno-stained for Ki67 (Yellow) and Rab7 (Magenta), Yellow boxes denote zoom-in areas shown in the row below. (B) 50ng/mL of Alexa Fluor-647 labelled EGF (Green) is added to organoids after 96h of growth, after 30min of incubation organoids were fixed and stained. Yellow boxes denote zoom-in areas shown in the row bellow with EGF-647 (Green) and Rab7 (Magenta). (C) Digital Lightsheet Microscopy was used to see EGF-647 endocytosis in an organoid crypt grown for 96h in NR medium. Images showing Cell Mask, Hoechst and EGF-647 every 10 minutes. Red triangles show cells protruding into the lumen. For more details see *Methods* and (Video1)

Video1. EGF-647 endocytosis in NR grown organoid crypt using Digital Light Sheet imaging.

References

Abud, H.E., W.H. Chan, and T. Jardé. 2021. Source and impact of the EGF family of ligands on intestinal stem cells. *Front. Cell Dev. Biol.* 9:685665.

Alshammari, Y., H. Ali, M.B. Assas, R. Alshammari, M. Assas, L. Koti, R. Nizam, and F. Al-Mulla. 2026. Reduced plasma epidermal growth factor levels reflect poor glycaemic status in type 2 diabetes. *Endocr. Connect.* 15.

Arteaga, C.L., and J.A. Engelman. 2014. ERBB receptors: from oncogene discovery to basic science to mechanism-based cancer therapeutics. *Cancer Cell*. 25:282–303.

Basak, O., J. Beumer, K. Wiebrands, H. Seno, A. van Oudenaarden, and H. Clevers. 2017. Induced quiescence of Lgr5+ stem cells in intestinal organoids enables differentiation of hormone-producing enteroendocrine cells. *Cell Stem Cell*. 20:177–190.

Baumdick, M., Y. Brüggemann, M. Schmick, G. Xouri, O. Sabet, L. Davis, J.W. Chin, and P.I.H. Bastiaens. 2015. EGF-dependent re-routing of vesicular recycling switches spontaneous phosphorylation suppression to EGFR signaling. *Elife*. 4:e12223.

Boretto, M., M.H. Geurts, S. Gandhi, Z. Ma, N. Staliarova, M. Celotti, S. Lim, G.-W. He, R. Millen, and E. Driehuis. 2024. Epidermal growth factor receptor (EGFR) is a target of the tumor-suppressor E3 ligase FBXW7. *Proceedings of the National Academy of Sciences*. 121:e2309902121.

Brändli, A.W., E.D. Adamson, and K. Simons. 1991. Transcytosis of epidermal growth factor. The epidermal growth factor receptor mediates uptake but not transcytosis. *Journal of Biological Chemistry*. 266:8560–8566.

Brüggemann, Y., L.S. Karajannis, A. Stanoev, W. Stallaert, and P.I.H. Bastiaens. 2021. Growth factor–dependent ErbB vesicular dynamics couple receptor signaling to spatially and functionally distinct Erk pools. *Sci. Signal.* 14:eabd9943.

Calafiore, M., Y.-Y. Fu, P. Vinci, V. Arnhold, W.Y. Chang, S.A. Jansen, A. Egorova, S. Takashima, J. Kuttiyara, and T. Ito. 2023. A tissue-intrinsic IL-33/EGF circuit promotes epithelial regeneration after intestinal injury. *Nat. Commun.* 14:5411.

Chen, C.-L., X. Yu, I.O.A. James, H. Zhang, J. Yang, A. Radulescu, Y. Zhou, and G.E. Besner. 2012. Heparin-binding EGF-like growth factor protects intestinal stem cells from injury in a rat model of necrotizing enterocolitis. *Laboratory investigation*. 92:331–344.

Childs, C.J., E.M. Holloway, C.W. Sweet, Y.-H. Tsai, A. Wu, A. Vallie, M.K. Eiken, M.M. Capeling, R.K. Zwick, and B. Palikuqi. 2023. EPIREGULIN creates a developmental niche for spatially organized human intestinal enteroids. *JCI Insight*. 8.

Deguchi, E., S. Lin, D. Hirayama, K. Matsuda, A. Tanave, K. Sumiyama, S. Tsukiji, T. Otani, M. Furuse, and A. Sorkin. 2024. Low-affinity ligands of the epidermal growth factor receptor are long-range signal transmitters in collective cell migration of epithelial cells. *Cell Rep.* 43.

Fisher, D.A., and J. Lakshmanan. 1990. Metabolism and effects of epidermal growth factor and related growth factors in mammals. *Endocr. Rev.* 11:418–442.

Freed, D.M., N.J. Bessman, A. Kiyatkin, E. Salazar-Cavazos, P.O. Byrne, J.O. Moore, C.C. Valley, K.M. Ferguson, D.J. Leahy, and D.S. Lidke. 2017. EGFR ligands differentially stabilize receptor dimers to specify signaling kinetics. *Cell*. 171:683–695.

Fujii, M., M. Matano, K. Toshimitsu, A. Takano, Y. Mikami, S. Nishikori, S. Sugimoto, and T. Sato. 2018. Human intestinal organoids maintain self-renewal capacity and cellular diversity in niche-inspired culture condition. *Cell Stem Cell*. 23:787–793.

He, G.-W., L. Lin, J. DeMartino, X. Zheng, N. Staliarova, T. Dayton, H. Begthel, W.J. van de Wetering, E. Bodewes, and J. van Zon. 2022. Optimized human intestinal organoid model reveals interleukin-22-dependency of paneth cell formation. *Cell Stem Cell*. 29:1333–1345.

Hu, H., H. Gehart, B. Artegiani, C. LÖpez-Iglesias, F. Dekkers, O. Basak, J. van Es, S.M.C. de Sousa Lopes, H. Begthel, and J. Korving. 2018. Long-term expansion of functional mouse and human hepatocytes as 3D organoids. *Cell*. 175:1591–1606.

Jardé, T., W.H. Chan, F.J. Rossello, T.K. Kahlon, M. Theocharous, T.K. Arackal, T. Flores, M. Giraud, E. Richards, and E. Chan. 2020. Mesenchymal niche-derived neuregulin-1 drives intestinal stem cell proliferation and regeneration of damaged epithelium. *Cell Stem Cell*. 27:646–662.

Jendrisek, G., D. Mesa, A. Conte, M.G. Malabarba, and S. Sigismund. 2026. Beyond the membrane: rethinking EGFR signaling in physiology and cancer. *Cellular and Molecular Life Sciences*.

Joshi, M.S., A. Stanoev, J. Huebinger, B. Soetje, V. Zorina, L. Roßmannek, K. Michel, S.A.H. Müller, and P.I.H. Bastiaens. 2023. The EGFR phosphatase RPTPγ is a redox-regulated suppressor of promigratory signaling. *EMBO J.* 42:e111806.

Langlands, A.J., A.A. Almet, P.L. Appleton, I.P. Newton, J.M. Osborne, and I.S. Näthke. 2016. Paneth cell-rich regions separated by a cluster of Lgr5+ cells initiate crypt fission in the intestinal stem cell niche. *PLoS Biol.* 14:e1002491.

Lemmetyinen, T.T., E.W. Viitala, L. Wartiovaara, T. Kaprio, J. Hagström, C. Haglund, P. Katajisto, T.C. Wang, E. Domènech-Moreno, and S. Ollila. 2023. Fibroblast-derived EGF ligand neuregulin 1 induces fetal-like reprogramming of the intestinal epithelium without supporting tumorigenic growth. *Dis. Model. Mech.* 16:dmm049692.

Mahe, M.M., E. Aihara, M.A. Schumacher, Y. Zavros, M.H. Montrose, M.A. Helmrath, T. Sato, and N.F. Shroyer. 2013. Establishment of gastrointestinal epithelial organoids. *Curr. Protoc. Mouse Biol.* 3:217–240.

Roepstorff, K., M.V. Grandal, L. Henriksen, S.L.J. Knudsen, M. Lerdrup, L. Grøvdal, B.M. Willumsen, and B. Van Deurs. 2009. Differential effects of EGFR ligands on endocytic sorting of the receptor. *Traffic*. 10:1115–1127.

Sato, T., J.H. Van Es, H.J. Snippert, D.E. Stange, R.G. Vries, M. Van Den Born, N. Barker, N.F. Shroyer, M. Van De Wetering, and H. Clevers. 2011a. Paneth cells constitute the niche for Lgr5 stem cells in intestinal crypts. *Nature*. 469:415–418.

Sato, T., D.E. Stange, M. Ferrante, R.G.J. Vries, J.H. Van Es, S. Van Den Brink, W.J. Van Houdt, A. Pronk, J. Van Gorp, and P.D. Siersema. 2011b. Long-term expansion of epithelial organoids from human colon, adenoma, adenocarcinoma, and Barrett's epithelium. *Gastroenterology*. 141:1762–1772.

Sato, T., R.G. Vries, H.J. Snippert, M. Van De Wetering, N. Barker, D.E. Stange, J.H. Van Es, A. Abo, P. Kujala, and P.J. Peters. 2009. Single Lgr5 stem cells build crypt-villus structures in vitro without a mesenchymal niche. *Nature*. 459:262–265.

Scharaw, S., M. Iskar, A. Ori, G. Boncompain, V. Laketa, I. Poser, E. Lundberg, F. Perez, M. Beck, and P. Bork. 2016. The endosomal transcriptional regulator RNF11 integrates degradation and transport of EGFR. *Journal of Cell Biology*. 215:543–558.

Schaudies, R.P., J. Grimes, D. Davis, R.K. Rao, and O. Koldovsky. 1989. EGF content in the gastrointestinal tract of rats: effect of age and fasting/feeding. *American Journal of Physiology-Gastrointestinal and Liver Physiology*. 256:G856–G861.

Schmick, M., and P.I.H. Bastiaens. 2014. The interdependence of membrane shape and cellular signal processing. *Cell*. 156:1132–1138.
Serra, D., U. Mayr, A. Boni, I. Lukonin, M. Rempfler, L. Challet Meylan, M.B. Stadler, P. Strnad, P. Papasaikas, and D. Vischi. 2019. Self-organization and symmetry breaking in intestinal organoid development. *Nature*. 569:66–72.
Shankaran, A., K. Prasad, S. Chaudhari, A. Brand, and K. Satyamoorthy. 2021. Advances in development and application of human organoids. *3 Biotech*. 11:257.
Sonntag, M.H., J. Ibach, L. Nieto, P.J. Verveer, and L. Brunsveld. 2014. Site-specific protection and dual labeling of human epidermal growth factor (hEGF) for targeting, imaging, and cargo delivery. *Chemistry–A European Journal*. 20:6019–6026.
Sprangers, J., I.C. Zaalberg, and M.M. Maurice. 2021. Organoid-based modeling of intestinal development, regeneration, and repair. *Cell Death Differ.* 28:95–107.
Stanoev, A., A. Mhamane, K.C. Schuermann, H.E. Grecco, W. Stallaert, M. Baumdick, Y. Brüggemann, M.S. Joshi, P. Roda-Navarro, and S. Fengler. 2018. Interdependence between EGFR and phosphatases spatially established by vesicular dynamics generates a growth factor sensing and responding network. *Cell Syst.* 7:295–309.
Sumigray, K.D., M. Terwilliger, and T. Lechler. 2018. Morphogenesis and compartmentalization of the intestinal crypt. *Dev. Cell*. 45:183–197.
Tallapragada, N.P., H.M. Cambra, T. Wald, S.K. Jalbert, D.M. Abraham, O.D. Klein, and A.M. Klein. 2021. Inflation-collapse dynamics drive patterning and morphogenesis in intestinal organoids. *Cell Stem Cell*. 28:1516–1532.
Tschumperlin, D.J., G. Dai, I. V Maly, T. Kikuchi, L.H. Laiho, A.K. McVittie, K.J. Haley, C.M. Lilly, P.T.C. So, and D.A. Lauffenburger. 2004. Mechanotransduction through growth-factor shedding into the extracellular space. *Nature*. 429:83–86.
van der Vaart, J., L. Bosmans, S.F. Sijbesma, K. Knoops, W.J. van de Wetering, H.G. Otten, H. Begthel, I.H.M. Borel Rinkes, J. Korving, and E.G.W.M. Lentjes. 2021. Adult mouse and human organoids derived from thyroid follicular cells and modeling of Graves' hyperthyroidism. *Proceedings of the National Academy of Sciences*. 118:e2117017118.
Wang, Y., Y. Guo, P. Wang, J. Liu, X. Zhang, Q. Liu, L. Wei, C. Xu, and J. Qin. 2025. An engineered human placental organoid microphysiological system in a vascular niche to model viral infection. *Commun. Biol.* 8:669.
Yang, L., X. Wang, X. Zhou, H. Chen, S. Song, L. Deng, Y. Yao, and X. Yin. 2025. A tunable human intestinal organoid system achieves controlled balance between self-renewal and differentiation. *Nat. Commun.* 16:315.
Yang, Y.-P., H. Ma, A. Starchenko, W.J. Huh, W. Li, F.E. Hickman, Q. Zhang, J.L. Franklin, D.P. Mortlock, and S. Fuhrmann. 2017. A chimeric Egfr protein reporter mouse reveals Egfr localization and trafficking in vivo. *Cell Rep.* 19:1257–1267.

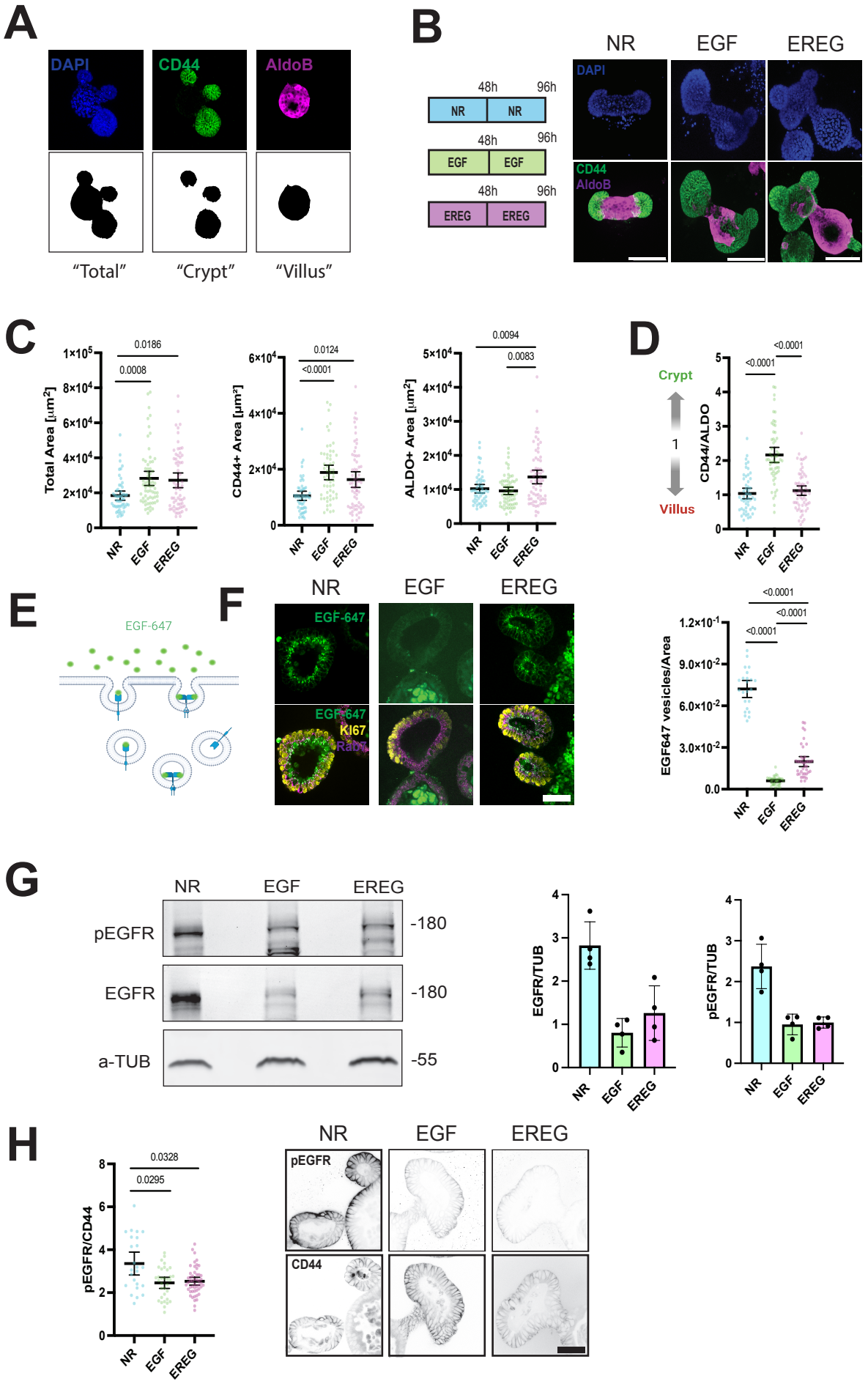
A
DAPI
CD44
AldoB
"Total"
"Crypt"
"Villus"
B
NR
EGF
EREG
48h
96h
DAPI
CD44
AldoB
C
Total Area [µm²]
CD44+ Area [µm²]
ALDO+ Area [µm²]
0.0186
0.0008
0.0124
<0.0001
0.0094
0.0083
D
Crypt
Villus
CD44/ALDO
<0.0001
E
EGF-647
F
EGF-647
KI67
Rab7
EGF647 vesicles/Area
G
pEGFR
EGFR
a-TUB
-180
-55
EGFR/TUB
pEGFR/TUB
H
pEGFR/CD44
0.0328
0.0295
pEGFR
CD44

Figure 1.

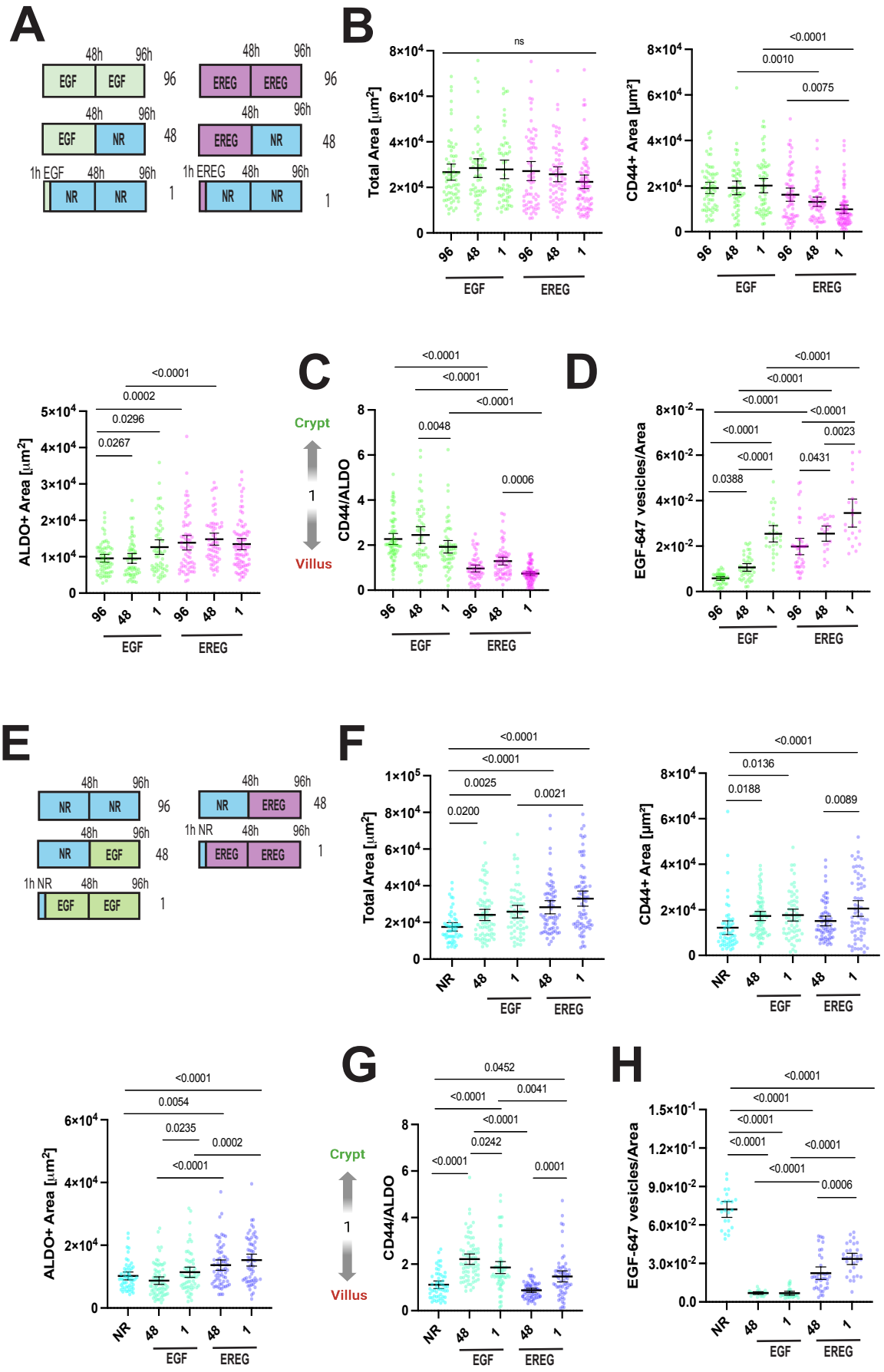
A
48h
96h
EGF
EGF
96
EREG
EREG
NR
48
1h EGF
1h EREG
1
B
Total Area [µm²]
CD44+ Area [µm²]
ns
<0.0001
0.0010
0.0075
EGF
EREG
C
ALDO+ Area [µm²]
CD44/ALDO
Crypt
Villus
0.0002
0.0296
0.0267
0.0048
0.0006
D
EGF-647 vesicles/Area
0.0388
0.0431
0.0023
E
1h NR
F
0.0025
0.0021
0.0200
0.0136
0.0188
0.0089
G
0.0452
0.0041
0.0242
0.0054
0.0235
H
0.0006

Figure 2.

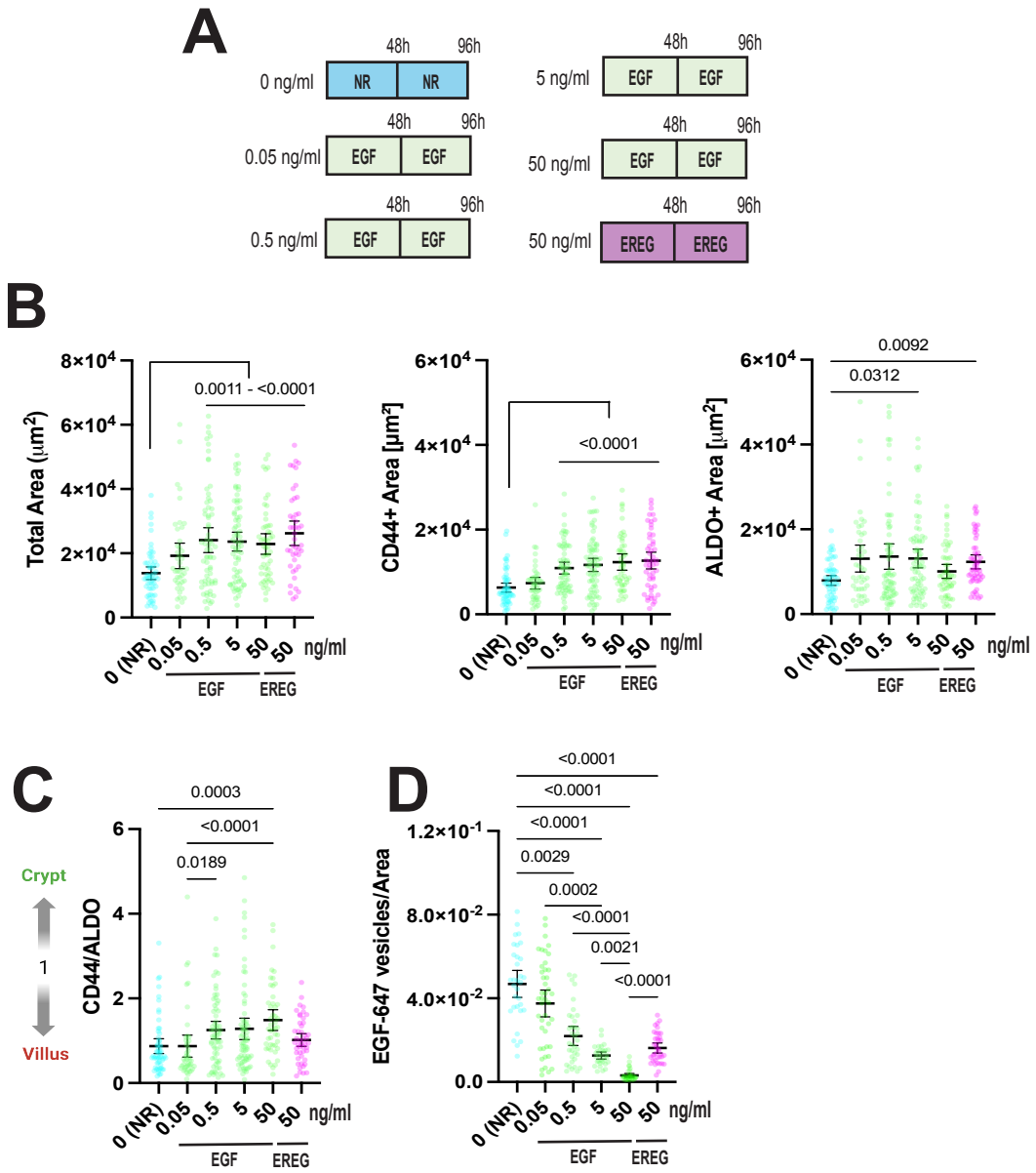
A
48h
96h
0 ng/ml
NR
NR
0.05 ng/ml
EGF
EGF
0.5 ng/ml
EGF
EGF
5 ng/ml
EGF
EGF
50 ng/ml
EGF
EGF
50 ng/ml
EREG
EREG
B
Total Area (μm²)
8×10⁴
6×10⁴
4×10⁴
2×10⁴
0
0.0011 - <0.0001
CD44+ Area [μm²]
6×10⁴
4×10⁴
2×10⁴
0
<0.0001
ALDO+ Area [μm²]
6×10⁴
4×10⁴
2×10⁴
0
0.0092
0.0312
0 (NR)
0.05
0.5
5
50
50
ng/ml
EGF
EREG
C
Crypt
1
Villus
CD44/ALDO
6
4
2
0
0.0003
<0.0001
0.0189
D
EGF-647 vesicles/Area
1.2×10⁻¹
8.0×10⁻²
4.0×10⁻²
0.0
<0.0001
<0.0001
<0.0001
0.0029
0.0002
<0.0001
0.0021
<0.0001

Figure 3.

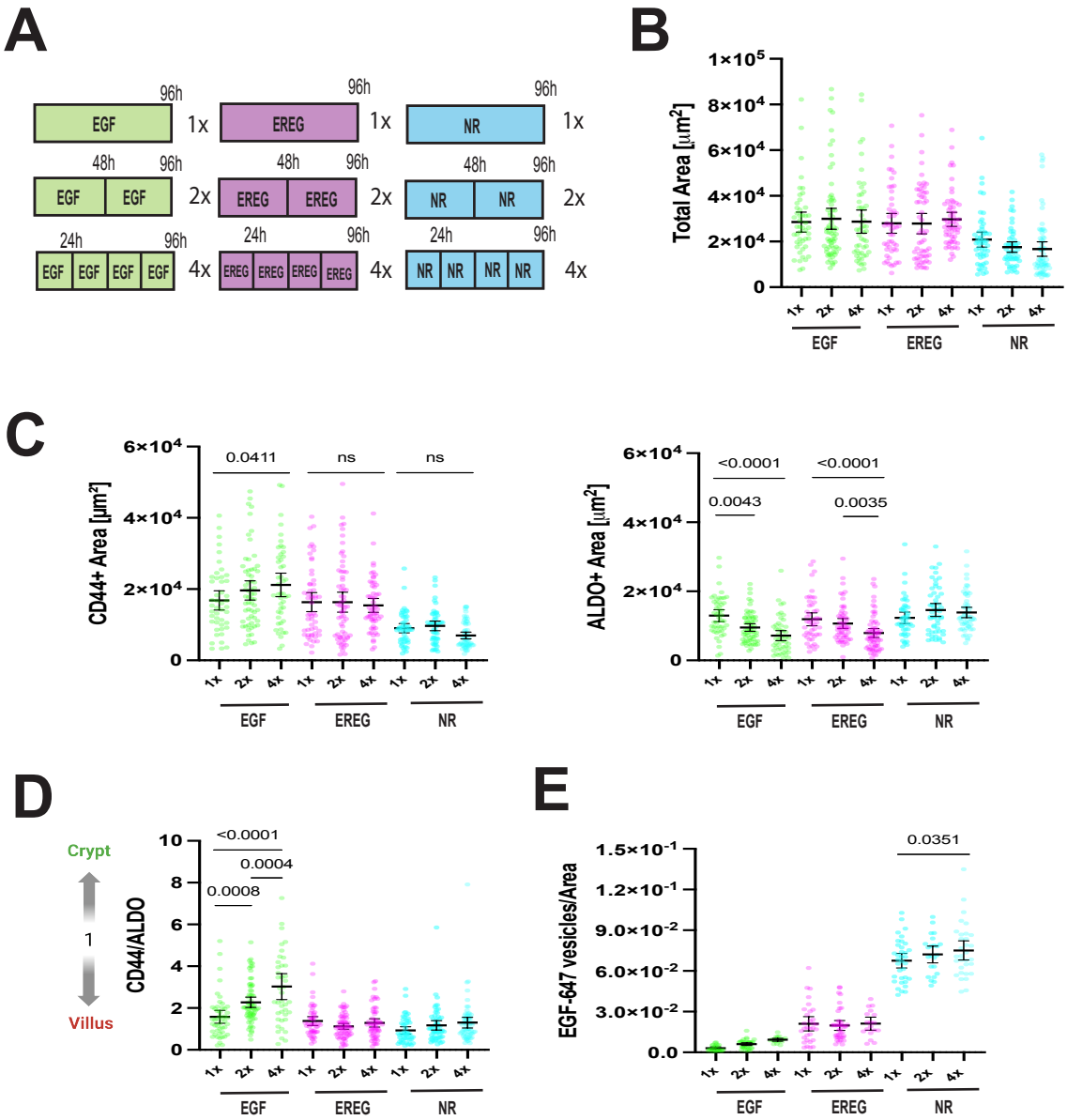
A
96h
EGF
1x
EREG
NR
48h
EGF EGF
EREG EREG
NR NR
2x
24h
EGF EGF EGF EGF
EREG EREG EREG EREG
NR NR NR NR
4x
B
Total Area [µm²]
1×10⁵
8×10⁴
6×10⁴
4×10⁴
2×10⁴
0
1x 2x 4x 1x 2x 4x 1x 2x 4x
EGF
EREG
NR
C
CD44+ Area [µm²]
6×10⁴
4×10⁴
2×10⁴
0
0.0411
ns
ns
ALDO+ Area [µm²]
<0.0001
<0.0001
0.0043
0.0035
D
Crypt
1
Villus
CD44/ALDO
10
8
6
4
2
0
<0.0001
0.0004
0.0008
E
EGF-647 vesicles/Area
1.5×10⁻¹
1.2×10⁻¹
9.0×10⁻²
6.0×10⁻²
3.0×10⁻²
0.0
0.0351

Figure 4.

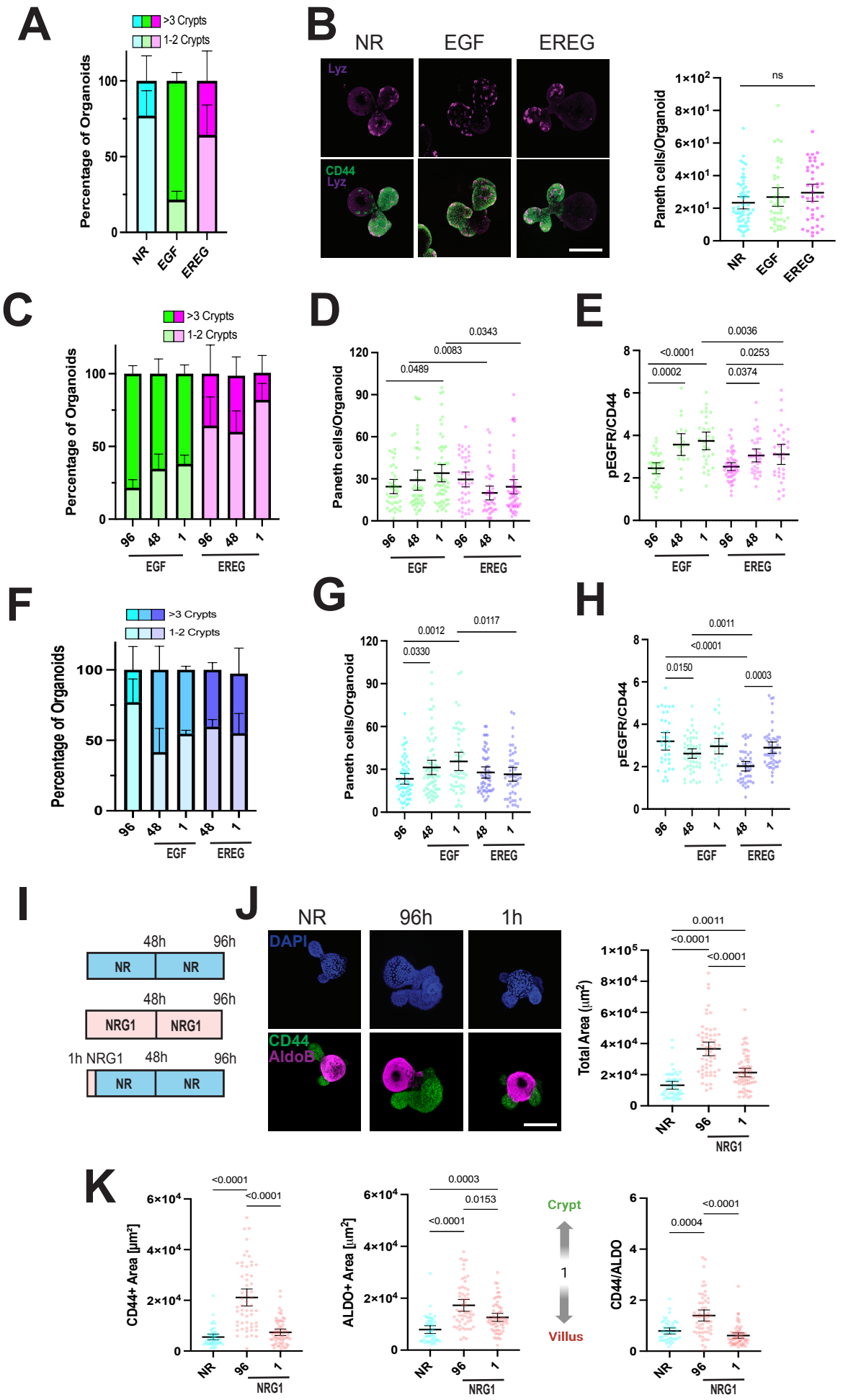
A
>3 Crypts
1-2 Crypts
Percentage of Organoids
NR
EGF
EREG
B
NR
EGF
EREG
Lyz
CD44
Lyz
Paneth cells/Organoid
ns
C
Percentage of Organoids
EGF
EREG
D
Paneth cells/Organoid
0.0343
0.0083
0.0489
E
pEGFR/CD44
0.0036
<0.0001
0.0253
0.0002
0.0374
F
Percentage of Organoids
G
Paneth cells/Organoid
0.0117
0.0012
0.0330
H
pEGFR/CD44
0.0011
<0.0001
0.0150
0.0003
I
48h
96h
NR
NRG1
1h NRG1
J
NR
96h
1h
DAPI
CD44
AldoB
Total Area (μm²)
0.0011
<0.0001
<0.0001
K
CD44+ Area [μm²]
<0.0001
<0.0001
ALDO+ Area [μm²]
0.0003
0.0153
<0.0001
Crypt
1
Villus
CD44/ALDO
<0.0001
0.0004

Figure S1.

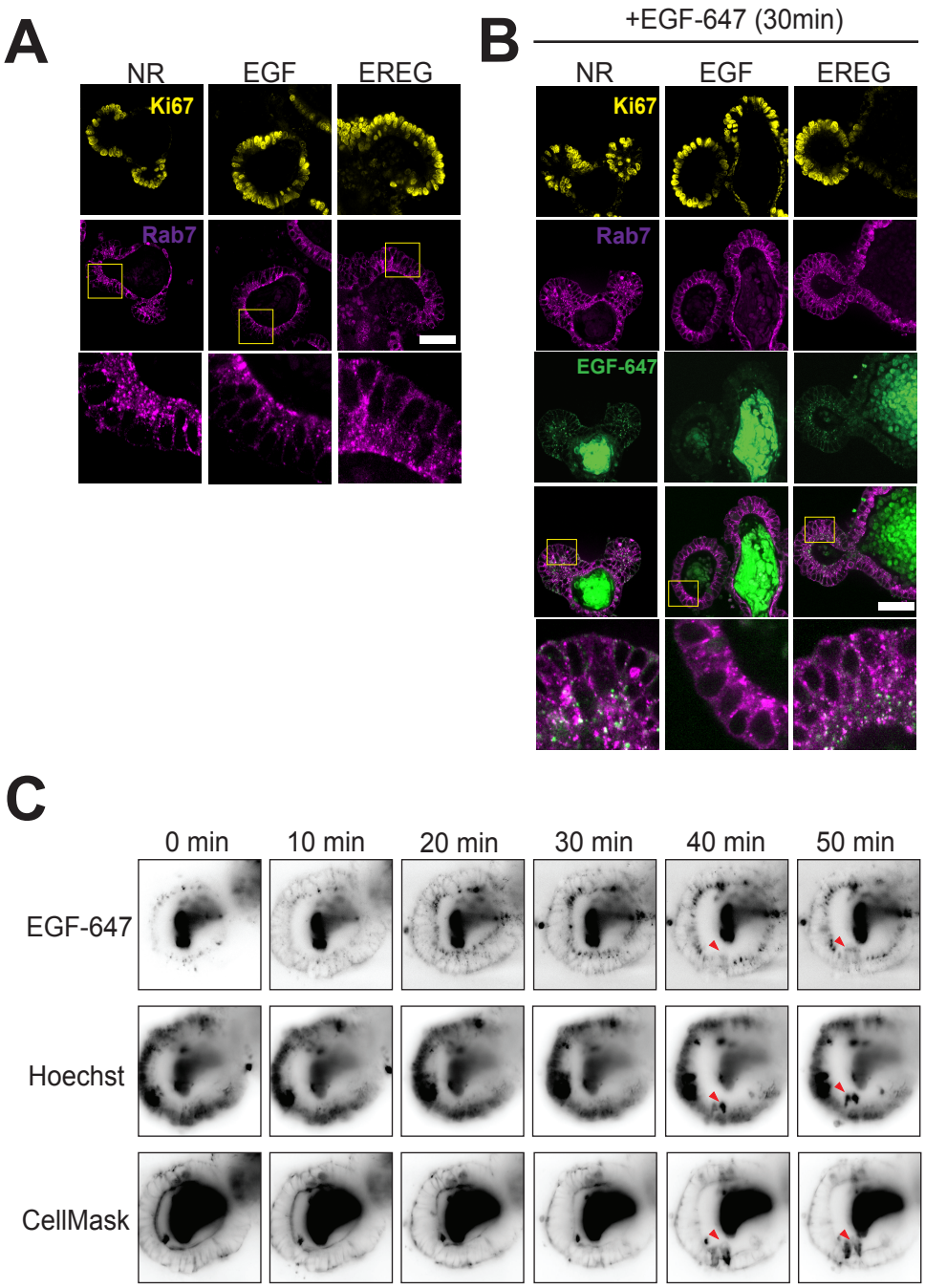
A
NR
EGF
EREG
Ki67
Rab7
B
+EGF-647 (30min)
NR
EGF
EREG
Ki67
Rab7
EGF-647
C
0 min
10 min
20 min
30 min
40 min
50 min
EGF-647
Hoechst
CellMask

Figure S2.

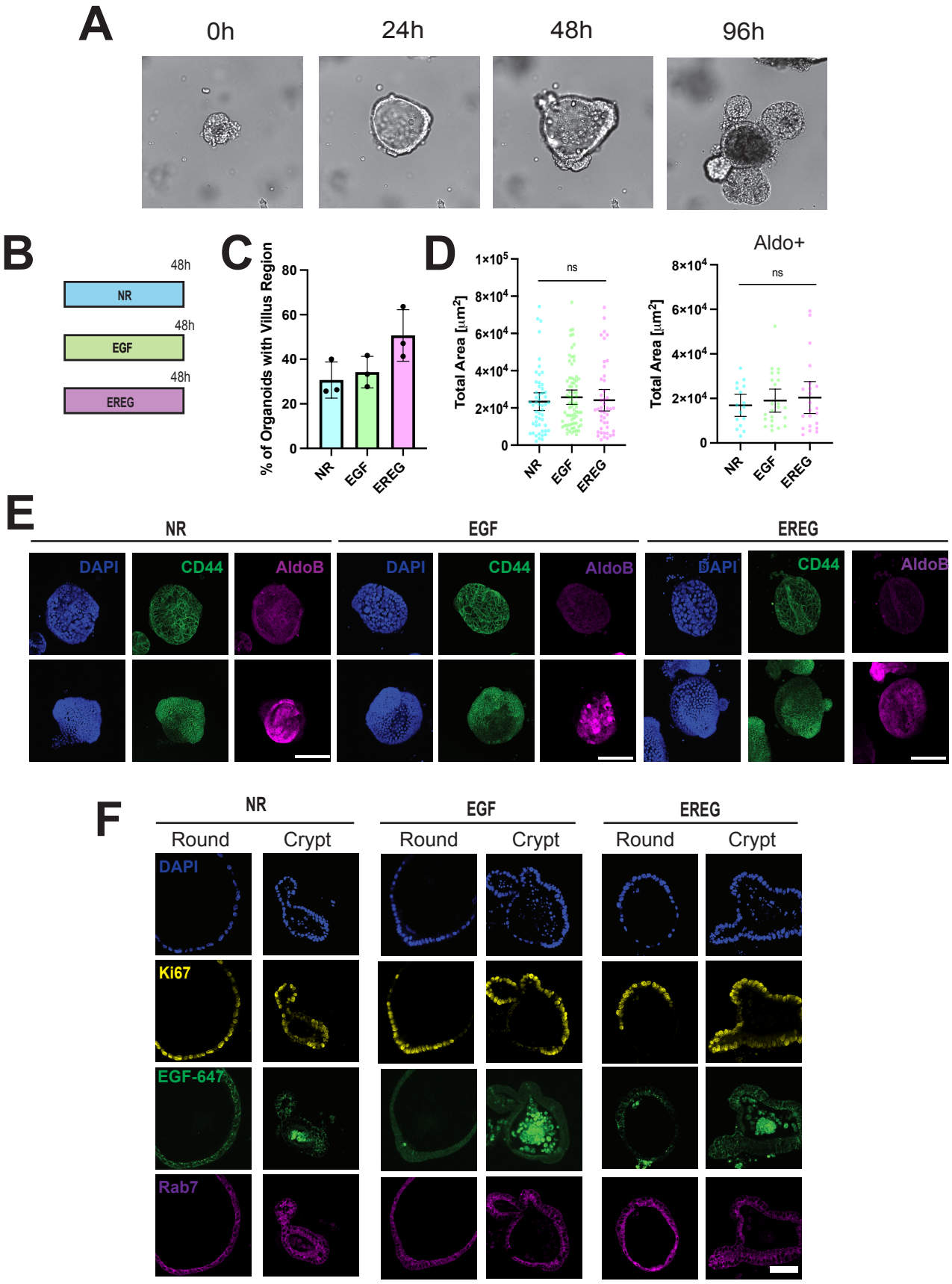
A
0h
24h
48h
96h
B
48h
NR
48h
EGF
48h
EREG
C
% of Organoids with Villus Region
80
60
40
20
0
NR
EGF
EREG
D
Total Area [µm²]
1×10⁵
8×10⁴
6×10⁴
4×10⁴
2×10⁴
0
ns
NR
EGF
EREG
Aldo+
Total Area [µm²]
8×10⁴
6×10⁴
4×10⁴
2×10⁴
0
ns
NR
EGF
EREG
E
NR
EGF
EREG
DAPI
CD44
AldoB
DAPI
CD44
AldoB
DAPI
CD44
AldoB
F
NR
EGF
EREG
Round
Crypt
Round
Crypt
Round
Crypt
DAPI
Ki67
EGF-647
Rab7

Figure S3.